Journal of
Applied Crystallography
ISSN 0021-8898

Received 27 April 2006
Accepted 15 August 2006

Analysis of polydisperse bubbles in the aluminium–hydrogen system using a size-dependent contrast

M. Paskevicius and C. E. Buckley*

Department of Applied Physics, Curtin University of Technology, Australia. Correspondence e-mail: c.buckley@curtin.edu.au

The characterization of hydrogen defects in an aluminium–hydrogen system was performed previously [Buckley *et al.* (2001). *J. Appl. Cryst.* **34**, 119–129] using small-angle scattering, inelastic neutron scattering and electron microscopy techniques. This analysis resulted in the determination of the relative change in lattice parameter as a result of hydrogen introduction into the Al matrix. However, this method relied on the average volume of the bubbles of hydrogen and also the pressure in a bubble of average volume. The characterization of the Al–H system has been improved by considering the size polydispersity of the hydrogen bubbles. The determination of a volume-fraction size distribution of the bubbles from small-angle scattering data has allowed a polydispersity analysis to be undertaken. A size-dependent contrast has been utilized in the modification of the volume-fraction size distribution into a more accurate form that accounts for varying concentrations of hydrogen within bubbles of different sizes. The determination of the size-dependent contrast is based upon an equation of state for molecular hydrogen which incorporates the compressibility of hydrogen under high pressures. The formation of alane (AlH_3) is also investigated, as it can be formed by the chemisorption of hydrogen in aluminium under high pressures. The polydispersity analysis has allowed a more accurate description of the Al–H system and can be applied to similar scattering systems where the scattering length density is not constant over the whole scattering size regime.

1. Introduction

Aluminium foils and single crystals were charged with hydrogen using a gas plasma method and electrochemical methods (Buckley *et al.*, 2001; Buckley & Birnbaum, 2002), resulting in the introduction of a large amount of hydrogen. It was hypothesized that the hydrogen did not enter the lattice as an interstitial solute, but instead formed an H-vacancy complex at the surface that diffused into the bulk and then clustered to form H_2 bubbles.

Both small- and ultra-small-angle neutron scattering (SANS, USANS) techniques were employed to study the nature and agglomeration of the H-vacancy complexes in the Al–H system (see Fig. 1) (Buckley *et al.*, 2001). Both the SANS and USANS investigations, along with transmission and scanning electron microscopy (TEM, SEM), revealed the existence of a large size distribution of hydrogen bubbles on the surface and in the bulk of the Al–H system (see Fig. 2).

The size distribution of hydrogen bubbles can be accurately determined by performing an in-depth analysis of the SANS and USANS scattering data. The size distribution can then be used to determine characteristics about the physical system, such as the total volume fraction of hydrogen bubbles in the material (or porosity), and the expansion of the aluminium lattice due to the introduction of hydrogen.

2. Experimental

The investigation herein is an extension of research performed by Buckley *et al.* (2001). The research involved the charging of aluminium foils (99.99% purity) and single crystals (99.999% purity) with hydrogen using a gas plasma method and electrochemical methods which resulted in hydrogen concentrations of up to 3000 atomic parts per million (a.p.p.m.) as measured by gas extraction and prompt gamma activation analysis (PGAA). There was zero change in lattice parameter (within experimental error) as measured by X-ray diffraction, which is unusual in comparison with other metals which exhibit large lattice expansions (Peisl, 1978).

Further structural investigation was undertaken using small-angle X-ray scattering (SAXS), SANS, USANS, TEM, SEM, inelastic neutron scattering (INS) and precision density measurements. Experimental details of the SANS and USANS are given here; details of the other experimental techniques can be found in the work by Buckley *et al.* (2001).

The SANS experiments were conducted on the aluminium foils using the 30 m SANS instrument at the National Institute

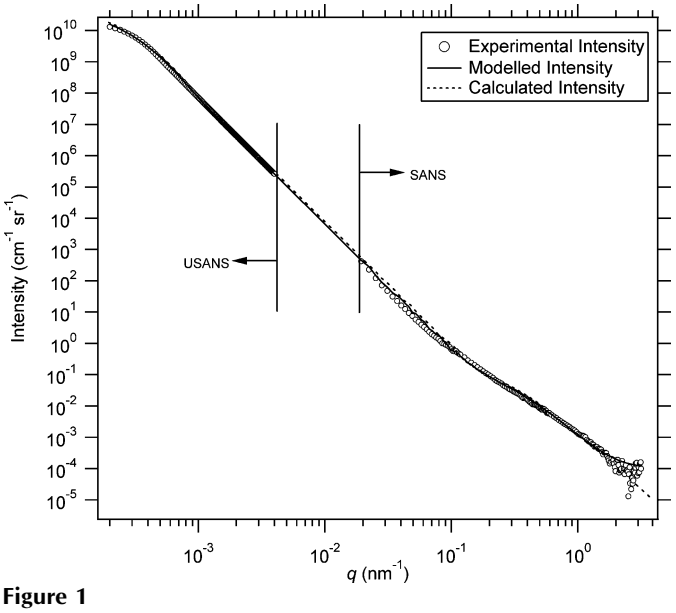

Figure 1
The differential small-angle scattering cross section over a wide q range as a result of SANS and USANS measurements. There were no data collected in the q range between the SANS and USANS data sets. For both sets of data, the experimental errors arise from the statistical errors of the measured intensities. The errors are ~1% at low q and ~10% at high q for the USANS data, and ~5% in the low-q region of the SANS data. Within experimental error, there is excellent agreement between the low-q region of the SANS data and the high-q region of the USANS measurements. The modelled intensity (solid line) was fit to the experimental data to obtain the volume-fraction size distribution, and the calculated intensity (broken line) was generated *via* equation (2) using the corrected volume-fraction size distribution given by equation (7) with the equation of state for molecular hydrogen.

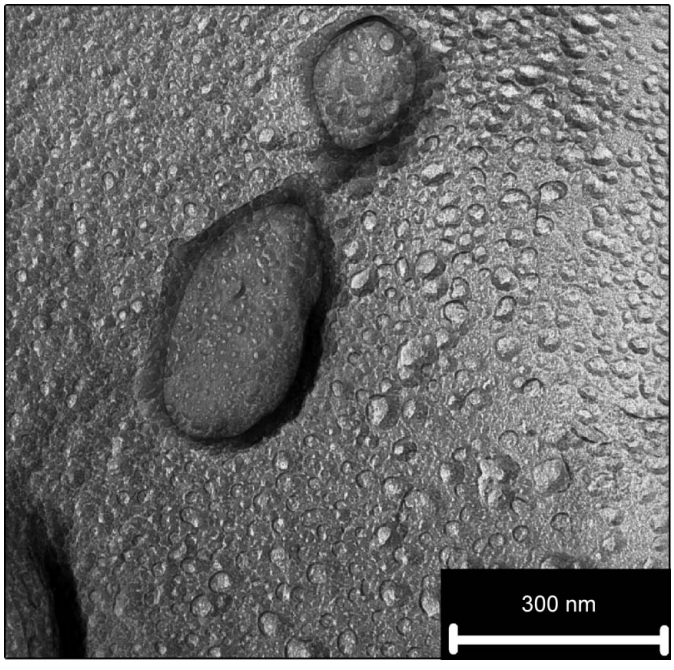

Figure 2
TEM micrograph of charged aluminium foil showing hydrogen bubbles with diameters in the range from 6 to 340 nm (Buckley *et al.*, 2001).

of Standards and Technology (NIST) Centre for Neutron Research (NCNR), using a wavelength of 0.8 ± 0.15 nm and three sample-to-detector distances (SDD), 1.3 m, 4.5 m and 13.17 m (Buckley & Birnbaum, 1998). The Intensity $I(q)$ was measured over the q range $0.019 < q$ (nm^{-1}) < 3.2, where $q = 4\pi \sin\theta/\lambda$ is the scattering vector, 2θ is the scattering angle and λ is the wavelength of incident radiation.

USANS was performed at the double-crystal diffractometer (DCD) at the Geesthacht Neutron Facility (GeNF) (Bellmann *et al.*, 1998) using a wavelength of 0.44244 ± 0.00036 nm. The absolute neutron wavelength of the DCD is determined by rocking a graphite crystal with a mosaic spread of 0.8° through the beam at the sample position. The resolution of the DCD is determined by the Darwin width of Si crystals, resulting in $\Delta\lambda/\lambda = 0.0018\%$. The scattering vector was in the range $1.0 \times 10^{-5} \leq q$ (nm^{-1}) $\leq 4.0 \times 10^{-3}$, but since the range $1 \times 10^{-5} \leq q$ (nm^{-1}) $\leq 1.3 \times 10^{-4}$ includes overlapping of the scattering with the primary beam, further analysis of the data was performed with $q_{\min} = 2 \times 10^{-4}$ nm^{-1}, which has been given previously (Agamalian *et al.*, 1997) as the minimum accessible scattering vector due to the resolution of the instrument. There is a q region ($q = 4.0 \times 10^{-3}$ to 1.94×10^{-2} nm^{-1}) where neither SANS nor DCD data were collected (see Fig. 1), because this q region was not accessible, due to insufficient scattering intensity at higher q values (DCD) and the limitations of the SANS experimental setup at lower q values. The DCD data cannot simply be linked to the SANS data, because DCD data are slit-height smeared while SANS is measured using a point-like collimation. Therefore, the DCD data are corrected for the smearing due to the DCD primary beam and also for multiple small-angle scattering (Schelten & Schmatz, 1980). The result of this correction produces the unsmeared scattering cross section shown in Fig. 1 (for the USANS data q

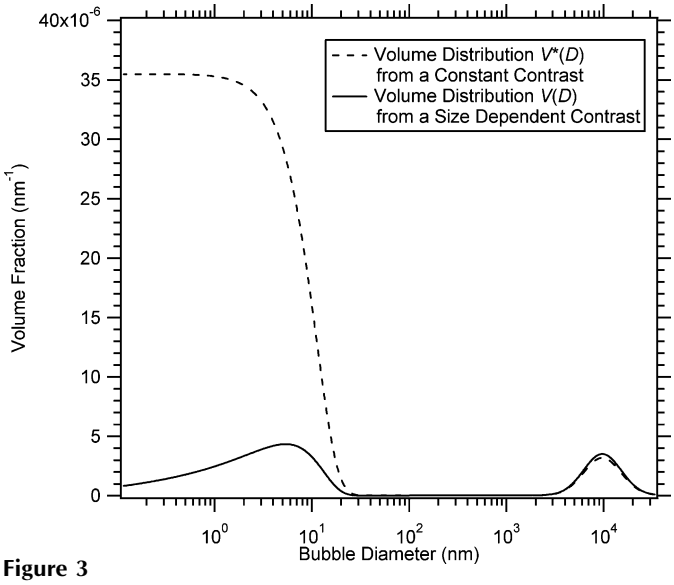

Figure 3
Calculated volume-fraction size distributions. $V^*(D)$ (broken line) was calculated using a constant contrast with *Irena*. $V(D)$ (solid line) was corrected by using a size-dependent contrast in the procedure discussed in this paper. The distributions represent the volume fraction of bubbles within the aluminium matrix.

$\leq 4.0 \times 10^{-3}$ nm^{-1}). Further details can be found in the work by Buckley *et al.* (2001).

3. Results and discussion

The scattering from a polydisperse system can be described using a constant scattering contrast, equation (1) (Ilavsky, 2005), or a size-dependent scattering contrast, equation (2):

$$I(q) = \frac{|\Delta\rho^*|^2}{C_b} \int_0^\infty |F(q, D)|^2 V_p(D) V^*(D)\, dD, \qquad (1)$$

$$I(q) = \frac{1}{C_b} \int_0^\infty |\Delta\rho(D)|^2 |F(q, D)|^2 V_p(D) V(D)\, dD, \qquad (2)$$

where $|\Delta\rho^*|^2$ is the constant scattering contrast, $|\Delta\rho(D)|^2$ is the size-dependent scattering contrast, C_b is the total volume fraction of particles (bubbles) in the system, $|F(q, D)|^2$ is the scattering form factor given by equation (3), $V_p(D)$ is the volume of a particle (bubble) and D is the particle size or bubble diameter (nm). It is convenient to define the volume-fraction size distribution (volume distribution) which has been calculated from a constant scattering contrast as $V^*(D)$, and that which is calculated from a size-dependent contrast to be $V(D)$.

The volume distribution of bubbles can be found (broken line in Fig. 3) by using the *Irena* package (Ilavsky, 2005) for the software application *Igor Pro* (Wavemetrics, Oregon, USA).

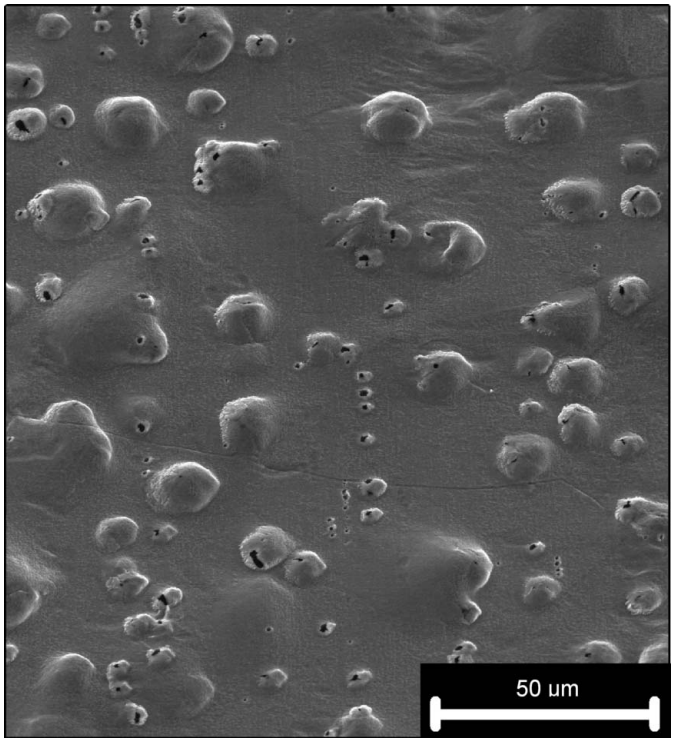

Figure 4
SEM micrograph of charged aluminium foil showing a range of hydrogen bubble sizes (3000 to 30000 nm) on the surface (Buckley *et al.*, 2001).

In order to determine this distribution of bubbles, *Irena* utilizes equation (1) with a constant scattering contrast. It should be noted that a constant scattering contrast would model a bubble distribution where bubbles of different sizes contain the same density of hydrogen. This is not the case in the Al–H system and instead the contrast is modified into a size-dependent form as discussed below, resulting in a corrected form of the volume distribution (solid line in Fig. 3). It should be noted that no extrapolation was necessary in the region shown in Fig. 1 between the SANS and USANS scattering data sets during the *Irena* fitting procedure. The bubbles were assumed to be spherical in the analysis, which is justified by studying the TEM and SEM micrographs (Figs. 2 and 4). A form factor for spherical particles was implemented in equation (1) according to (Guinier & Fournet, 1955):

$$|F(q, D)|^2 = \left[3\frac{\sin(qD/2) - (qD/2)\cos(qD/2)}{(qD/2)^3}\right]^2. \qquad (3)$$

The volume distribution $V^*(D)$, given by *Irena* (broken line in Fig. 3), can be expressed as the sum of Gaussian and log-normal distributions as follows (nm^{-1}):

$$\begin{aligned} V^*(D) &= V^*_{\text{Gaussian}}(D) + V^*_{\text{lognormal}}(D) \\ &= \left\{ y_0 + A_0 \exp\left[-\left(\frac{D - x_0}{w_0} \right)^2 \right] \right\} \\ &\quad + \left\{ y_1 + A_1 \exp\left[-\left(\frac{\ln(D/x_1)}{w_1} \right)^2 \right] \right\}, \end{aligned} \qquad (4)$$

where $y_0 = 21.0 \times 10^{22}$, $A_0 = 35.4 \times 10^{-6}$, $x_0 = 0.2$, $w_0 = 11.0$, $y_0 = 40.8 \times 10^{-9}$, $A_1 = 31.6 \times 10^{-7}$, $x_1 = 9670$, $w_1 = 0.630$, and D is in nm.

The calculated volume distribution $V^*(D)$ (broken line in Fig. 3) does not appear to reflect the physical Al–H system accurately because such a large contribution to the total volume of bubbles in $V^*(D)$ is made by bubbles smaller than 10 nm. It can be seen from Fig. 2 that a large number of bubbles smaller than 10 nm are present, but their contribution to the volume of the system is not expected to be as large as that given in Fig. 3. A larger contribution to the volume of the bubbles is also expected from bubbles between 3000 and 30000 nm, as shown in Fig. 4. Further evidence for bubbles from nm to µm size in the bulk can be found in the work by Buckley *et al.* (2001). It is thereby suggested that the inconsistency in the volume distribution in Fig. 3 (broken line) can be explained as a result of using a constant scattering contrast in a system which requires the implementation of a size-dependent scattering contrast. The scattering system is complicated because there are scattering particles (bubbles) which consist of H_2 molecules, which in turn control the degree of the scattering. A problem arises because the density of hydrogen inside each bubble is not constant across the bubble size distribution.

A distribution of hydrogen densities can be calculated, for the purpose of forming a size-dependent contrast, when the hydrogen bubbles are assumed to be spherical. The gaseous hydrogen (H_2) present in the bubbles is under different

Table 1
Coefficients for equations (8)–(11) for pressure (bar), molar volume ($cm^3\ mol^{-1}$) and temperature (K).

α_0	2.9315	b_5	−0.12385414
α_1	-1.531×10^{-3}	b_6	9.8570583×10^{-3}
α_2	4.154×10^{-6}	b_7	$-4.1153723 \times 10^{-4}$
b_0	20.285	b_8	7.02499×10^{-6}
b_1	−7.44171	a_1	19.599
b_2	7.318565	a_2	−0.8946
b_3	−3.463717	a_3	−18.608
b_4	0.87372903	a_4	2.6013

pressures for bubbles of various sizes. The pressure of hydrogen inside a spherical bubble of diameter D is given by (Buckley *et al.*, 2001)

$$p(D) = 4\gamma/D, \tag{5}$$

where $\gamma = 0.86\ N\ m^{-1}$ is the surface tension in Al.

Each hydrogen bubble of a different size in the aluminium matrix is under a different pressure, and the pressure controls the density of the hydrogen gas inside the bubbles. The degree of scattering that each bubble induces is a function of the amount of hydrogen present. Because there is a relationship between the size of the bubbles and the density of hydrogen, the scattering system cannot be described by a constant scattering contrast. The contrast must instead take a size-dependent form that is given by (Carsughi, 1994)

$$\begin{aligned} |\Delta\rho(D)|^2 &= |\rho_m - \rho_b(D)|^2 \\ &= \left|\frac{b_{Al}}{v_{Al}} - 2\rho_{H_2}(D)b_H\right|^2, \end{aligned} \tag{6}$$

where ρ_m is the scattering length density of the Al matrix, $\rho_b(D)$ is the size-dependent scattering length density of the bubbles, $b_{Al} = 0.3446 \times 10^{-12}$ cm is the scattering length of aluminium, $v_{Al} = 1.66 \times 10^{-23}\ cm^3$ is the atomic volume of aluminium, $b_H = -0.3740 \times 10^{-12}$ cm is the scattering length of a hydrogen atom, and $\rho_{H_2}(D) = N_{H_2}(D)/V_p(D)$ is the number volume density of molecular hydrogen present in a bubble of volume $V_p = \pi D^3/6$ and diameter D. $N_{H_2}(D)$ is the number of hydrogen molecules in a bubble of diameter D. The factor 2 is introduced in equation (6) because there are two hydrogen atoms for every H_2 molecule.

The size-dependent contrast given by equation (6) can be applied to the original volume distribution $V^*(D)$ in order to generate a corrected form of the volume distribution $V(D)$ as follows (Carsughi, 1994):

$$V(D) = \frac{|\Delta\rho^*|^2 V^*(D)}{|\Delta\rho(D)|^2}, \tag{7}$$

where $V(D)$ is the corrected volume distribution which incorporates the size-dependent contrast, $|\Delta\rho^*|^2 = 4.7961 \times 10^{20}\ cm^{-4}$ is the constant contrast, $V^*(D)$ is the original volume distribution, and $|\Delta\rho(D)|^2$ is the size-dependent contrast.

The corrected volume distribution can be calculated when the amount of hydrogen in each bubble is known. This can be achieved *via* an equation of state (EOS) for protium (H_2) developed by Hemmes *et al.* (1986) and given by McLennan & Gray (2004) as

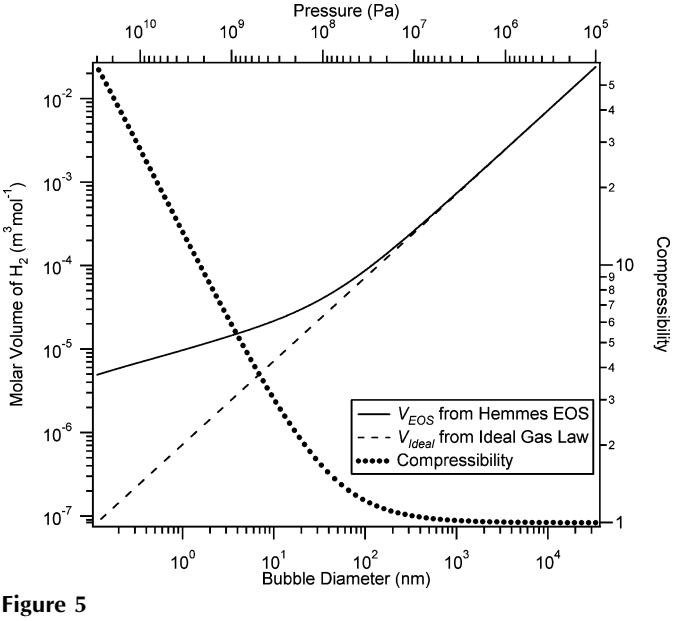

Figure 5
The molar volume of hydrogen at 298.15 K and at pressures encountered in the hydrogen bubbles. The molar volume has been numerically calculated according to the equation of state (V_{EOS}) as given by Hemmes *et al.* (1986) and according to the ideal gas law (V_{Ideal}). The compressibility is also shown, which is the volume ratio $Z = V_{EOS}/V_{Ideal}$.

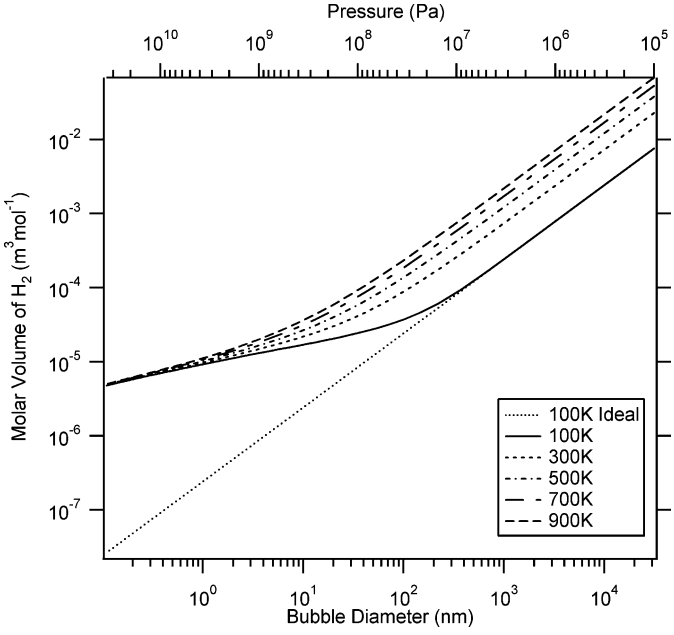

Figure 6
The molar volume of hydrogen at typical temperatures, numerically calculated from the equation of state given by Hemmes *et al.* (1986). The molar volume as calculated from the ideal gas law at 100 K is also shown for comparison.

$$\left[p + \frac{a(p)}{V_{\mathrm{EOS}}^{\alpha(T)}}\right]\left[V_{\mathrm{EOS}} - b(p)\right] = RT, \tag{8}$$

where

$$a(p) = \exp\left\{a_1 + a_2 \ln(p) - \exp\left[a_3 + a_4 \ln(p)\right]\right\}, \tag{9}$$

$$b(p) = \begin{cases} \sum_{i=0}^{8} b_i \ln(p)^i & (p \geq 100 \text{ bar}), \\ b\,(100 \text{ bar}) & (p < 100 \text{ bar}), \end{cases} \tag{10}$$

$$\alpha(T) = \begin{cases} \alpha_0 + \alpha_1 T + \alpha_2 T^2 & (T \leq 300 \text{ K}), \\ \alpha\,(300 \text{ K}) & (T > 300 \text{ K}), \end{cases} \tag{11}$$

where $p > 1$ bar (1 bar = 0.1 MPa), V_{EOS} is the molar volume of H_2, R = 83.14472 bar cm^3 K^{-1} mol^{-1} (R = 8.314472 J K^{-1} mol^{-1} in SI units) is the gas constant, T is the temperature, and the coefficients are given in Table 1.

The EOS given by equation (8) was solved numerically to determine the molar volume of hydrogen as a function of pressure and constant temperature T = 298.15 K. A comparison between the molar volumes given by the EOS and ideal gas law ($V_{\mathrm{Ideal}} = RT/p$) can be seen in Fig. 5 at 298.15 K and in Fig. 6 as a function of temperature.

The number of moles of hydrogen (H_2) per bubble of diameter D can be found *via* (McLennan & Gray, 2004)

$$n_{\mathrm{H_2}}(D) = \frac{p(D)V_{\mathrm{p}}(D)}{Z(D)RT}, \tag{12}$$

where $Z(D)$ is the compressibility, given as the ratio $V_{\mathrm{EOS}}(D)/V_{\mathrm{Ideal}}(D)$ between the EOS and ideal molar volumes, respectively.

The number of hydrogen (H_2) molecules $N_{\mathrm{H_2}}(D)$ per bubble can therefore be determined by

$$N_{\mathrm{H_2}}(D) = n_{\mathrm{H_2}}(D) \times 6.022 \times 10^{23}. \tag{13}$$

Hence the number volume density of molecular hydrogen per bubble of diameter D used in equation (5) is given by

$$\rho_{\mathrm{H_2}}(D) = \frac{N_{\mathrm{H_2}}(D)}{V_{\mathrm{p}}(D)}. \tag{14}$$

The size-dependent contrast can then be expressed *via* equation (6) as shown in Fig. 7.

When the size-dependent contrast is applied to the original volume distribution $V^*(D)$ given by the broken line in Fig. 3 *via* equation (7), a corrected volume distribution $V(D)$ is generated as shown by the solid line in Figs. 3 and 8. The corrected bubble volume distribution can be compared with the TEM micrograph shown in Fig. 2. Bubbles with diameters in the ranges of ~3–30 nm are visible in Fig. 2; these have a strong correlation with the corrected distribution that has a peak at ~5 nm. It should be noted that the larger bubbles (~150 nm) present in Fig. 2 are not represented by a significant peak in the volume distributions. This implies that bubbles of this size make up a small fraction of the total bubble volume distribution.

A significant proportion of the bubble volume-fraction size distribution (solid line in Fig. 8) arises from bubbles with diameters of ~3000–30000 nm. This result can be verified by reviewing the SEM micrograph in Fig. 4, which shows the existence of bubbles in this size range. It is apparent that the volume distribution $V(D)$, which has been corrected by utilizing a size-dependent contrast (solid line in Figs. 3 and 8), provides a more accurate description of the system of scat-

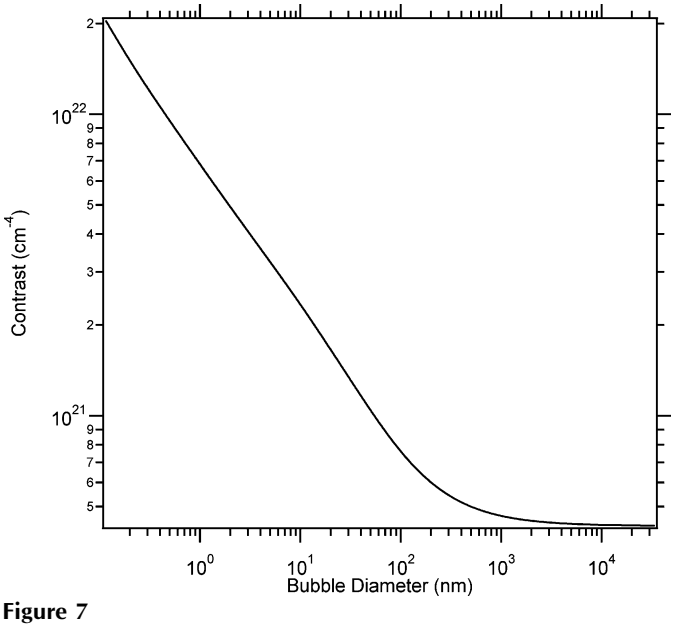

Figure 7
The size-dependent contrast, which is a function of the density of hydrogen within the bubbles in the aluminium matrix.

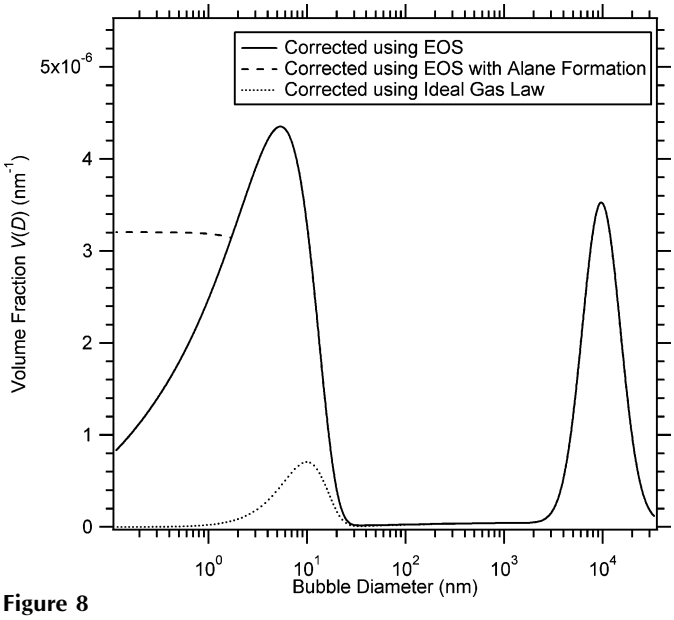

Figure 8
Bubble volume-fraction size distributions, which have all been corrected to include the effect of a size-dependent contrast. The solid line was calculated with the equation of state and the dotted line was calculated with the ideal gas law. The broken line reflects the effect that alane formation would have on the equation of state volume distribution if it were formed with more than 2 GPa pressure.

terers than the uncorrected volume distribution $V^*(D)$ given by the broken line in Fig. 3.

It is apparent from Fig. 5 that small hydrogen bubbles in the aluminium matrix are under very high pressures. In fact, the pressure in bubbles smaller than $\sim$2 nm is high enough (> 2 GPa) for the system to have initiated the chemisorption of molecular hydrogen into aluminium to form alane under moderate temperatures (> 473 K) (Baranowski & Tkacz, 1983; Konovalov & Bulychev, 1995) as follows:

$$\mathrm{Al(s)} + \tfrac{3}{2}\mathrm{H_2(g)} \leftrightarrow \mathrm{AlH_3(s)}. \qquad (15)$$

The formation of alane within small hydrogen bubbles in aluminium has been suggested previously (Ono *et al.*, 1991) where the bubbles collapsed, becoming disk-shaped as a result of losing hydrogen pressure. The collapse led to lattice defects around the bubbles which caused surrounding lattice distortions as viewed by TEM (Ono *et al.*, 1991). The small bubbles (< 2 nm) which would initially have hydrogen pressures greater than 2 GPa (see Fig. 5) would allow for some of the hydrogen inside each of these bubbles to react with the aluminium *via* equation (15) forming alane. This would result in a gas loss inside the bubble which would lower the pressure inside the bubble until it drops below 2 GPa when the reaction could no longer progress. This means that all bubbles below 2 nm would have a constant 2 GPa hydrogen pressure if alane was assumed to be formed.

The bubble volume-fraction size distribution that has been corrected to include the effect of a size-dependent contrast $V(D)$ (solid line in Fig. 8) can be manipulated to demonstrate the resultant volume distribution if alane is assumed to be formed under high pressures (> 2 GPa). It can be seen from the broken line in Fig. 8 that the volume distribution changes significantly for small bubbles, < 2 nm, if the formation of alane is considered. The difference between the size distributions in Fig. 8 (broken and solid lines) is due to small bubbles (< 2 nm) being at a lower pressure (2 GPa) if alane has been formed. The fact that the bubbles are at a lower pressure after alane formation means that there would be a lower number of moles of hydrogen in the small bubbles compared with the amount in these same bubbles before alane formation. This results in $V(D)$ being almost constant for bubble diameters < 2 nm when alane forms (see broken line in Fig. 8).

The bubble volume-fraction size distribution $V(D)$ that is given in Fig. 8 by the solid line has been corrected to include the effect of a size-dependent contrast. The equation of state given by equation (8) was used to determine the molar volume of hydrogen when this distribution was calculated so that it was accurate for the bubbles which are under high pressures. This volume distribution provides a good description of small bubbles under high pressure, which is not the case if the ideal gas law is used instead of the equation of state (dotted line in Fig. 8). The discrepancy is due to an over correction to the volume fraction of the smaller bubbles because of the ideal gas law's inaccuracies at high pressures.

The validity of the final bubble volume-fraction size distribution (solid line in Fig. 8) can be verified from the convolution of the size-dependent contrast, spherical form factor, particle volume and corrected volume distribution *via* equation (2). The reconstructed scattering pattern given by equation (2) is shown by the broken line in Fig. 1. The calculated scattering intensity provides a good fit to the experimental scattering data indicating that the corrected volume-fraction size distribution is accurate.

The volume-fraction size distribution can be used to provide additional information about the scattering system. The total volume fraction of the bubbles can be determined *via* (Jemian *et al.*, 1991)

$$\int V(D)\,\mathrm{d}D = C_\mathrm{b} \qquad (16)$$

where $C_\mathrm{b} = 0.043 = 4.3\%$ is the percentage of volume taken up by the H_2 bubbles in the Al matrix (or the porosity); this value is comparable with the result found by Buckley *et al.* (2001) as $(3.9 \pm 0.3) \times 10^{-2}$.

The change in the aluminium lattice parameter can be calculated as follows (Buckley *et al.*, 2001):

$$\delta a/a_0 = \frac{(3B + 4\mu)}{(3B)^2} \int_{D_\mathrm{min}}^{D_\mathrm{max}} V(D)p(D)\,\mathrm{d}D, \qquad (17)$$

where B = 77 GPa is the bulk modulus of Al, μ = 26.5 GPa is the shear modulus of Al, and D_min and D_max are the lower and upper limits of the size distribution.

The change in lattice parameter is given by equation (17) as $\delta a/a_0 = 3.7 \times 10^{-7}$. The change in lattice parameter calculated theoretically by Buckley *et al.* (2001) as $(2.3 \pm 0.2) \times 10^{-6}$ is over five times larger than the value calculated herein. This difference is due to the lack of polydispersity in the analysis given by Buckley *et al.* (2001). In equation (17), the change in lattice parameter is determined by summing the product of the volume and pressure of each bubble of a different size. This method produces a different result to only multiplying the average volume with the pressure in a bubble of average volume as performed by Buckley *et al.* (2001). The change in lattice parameter is more accurate when the polydispersity of the hydrogen bubbles is taken into account. However, the theoretical values for the change in lattice parameter calculated in this paper and by Buckley *et al.* (2001) both agree with the experimental change in lattice parameter, which was zero within experimental error.

4. Conclusion

A size-dependent scattering contrast was employed to modify the volume distribution of hydrogen bubbles in aluminium. The modification provided a volume distribution which more accurately reflected the bubble sizes observed with SEM and TEM. The calculation of the size-dependent contrast involved the implementation of an equation of state which more accurately modelled high hydrogen pressures compared with the ideal gas law. The formation of alane (AlH_3) was also considered in smaller bubbles which are under high enough

pressures to have allowed the chemisorption of hydrogen into aluminium. The corrected size distribution has been utilized in determining the total volume fraction of bubbles in the aluminium matrix and the change in the lattice parameter due to the introduction of hydrogen.

M. Paskevicius would like to thank the Australian government for the granting of an Australian Post Graduate Award with Stipend (APAWS), and the Australian Institute of Nuclear Science and Engineering (AINSE) for the granting of a postgraduate research award (PGRA).

References

Agamalian, M., Wignall, G. D. & Triolo, R. (1997). *J. Appl. Cryst.* **30**, 345–352.
Baranowski, B. & Tkacz, M. (1983). *Z. Phys. Chem. Neue. Fol.* **135**, 27–38.
Bellmann, D., Klatt, M., Kampmann, R. & Wagner, R. (1998). *Physica B*, **241–243**, 71–73.
Buckley, C. E. & Birnbaum, H. K. (1998). *Physica B*, **241–243**, 344–346.
Buckley, C. E. & Birnbaum, H. K. (2002). *J. Alloys Compd.* **330–332**, 649–653.
Buckley, C. E., Birnbaum, H. K., Lin, J. S., Spooner, S., Bellmann, D., Staron, P., Udovic, T. J. & Hollar, E. (2001). *J. Appl. Cryst.* **34**, 119–129.
Carsughi, F. (1994). *J. Appl. Cryst.* **27**, 326–329.
Guinier, A. & Fournet, G. (1955). *Small-Angle Scattering of X-rays*, pp. 5–82. New York: John Wiley.
Hemmes, H., Driessen, A. & Griessen, R. (1986). *J. Phys. C Solid State Phys.* **19**, 3571–3585.
Ilavsky, J. (2005). *Irena 2 SAS Modelling Macros*, Advanced Photon Source, Argonne National Laboratory.
Jemian, P. R., Weertman, J. R., Long, G. G. & Spal, R. D. (1991). *Acta Metall. Mater.* **39**, 2477–2487.
Konovalov, S. K. & Bulychev, B. M. (1995). *Inorg. Chem.* **34**, 172–175.
McLennan, K. G. & Gray, E. M. (2004). *Meas. Sci. Technol.* **15**, 211–215.
Ono, K., Kino, T., Furuno, S., Hojou, K., Izui, K., Mizuno, K. & Ito, K. (1991). *J. Nucl. Mater.* **183**, 154–160.
Peisl, H. (1978). *Hydrogen in Metals I, Topics in Applied Physics*, Vol. 28, edited by G. Alefeld & J. Volkl, pp. 53–74. Berlin: Springer.
Schelten, J. & Schmatz, W. (1980). *J. Appl. Cryst.* **13**, 385–390.